Journal of Alloys and Compounds 491 (2010) 416–419

Contents lists available at ScienceDirect

Journal of Alloys and Compounds

journal homepage: www.elsevier.com/locate/jallcom

Electrical conductivity studies on the LSGM–CGO composite electrolytes

Seung Hwan Jo[1], P. Muralidharan[1], Do Kyung Kim*

Department of Materials Science and Engineering, Korea Advanced Institute of Science and Technology (KAIST), 335 Gwahangno, Yuseong-gu, Daejeon 305-701, Republic of Korea

ARTICLE INFO

Article history:
Received 15 September 2009
Accepted 26 October 2009
Available online 31 October 2009

Keywords:
Composite materials
Fuel cells
Chemical synthesis
Sintering
Ionic conduction
Grain boundaries
Electrochemical impedance spectroscopy
X-ray diffraction

ABSTRACT

The composite electrolytes x mol% $La_{0.8}Sr_{0.2}Ga_{0.8}Mg_{0.2}O_{3-\delta}$ (LSGM)–$(100-x)$ mol% $Ce_{0.9}Gd_{0.1}O_{1.95}$ (CGO), where $x = 0$, 10, 20 and 50, were synthesized via a mechanical milling followed by a solid state reaction method. Powder X-ray diffraction patterns confirmed the presence of major phases of LSGM and CGO in the composites sintered at 1450 °C for 10 h. A dense grain morphology was recognized from the scanning electron microscopy images of the polished surface of the sintered pellets. The composite of 10 mol% LSGM–CGO (LC10-90) showed an improved electrical conductivity compared with a pristine CGO (LC0-100) electrolyte. The composites electrolytes with increasing concentration of LSGM above 10 mol% in the CGO matrix exhibited a lowering of electrical conductivity. On the other hand, the homogenously dispersed LSGM phase in the CGO matrix was effective to expand the electrolytic domain region toward low oxygen partial pressures (PO_2) compared with the pristine CGO electrolyte.

1. Introduction

Recent developments aim at the solid electrolytes with high ionic conductivity and low electronic conductivity under low oxygen partial pressures (PO_2) to maintain low ohmic loss at reduced operating temperatures (500–700 °C) for the commercialization of intermediate-temperature solid oxide fuel cells (IT-SOFCs). To date, conventionally used solid electrolytes with high ionic conductivity consist of fluorite-structured stabilized zirconia (YSZ), which requires high operating temperature above 800–1000 °C. Therefore, serious attention has been paid to finding alternative electrolytes for IT-SOFCs, which has led to the development of alternative fluorite and perovskite structures, including doped ceria and doped lanthanum gallate, respectively [1,2]. However, the application of doped ceria has been limited by the narrow electrolytic domain due to the change in oxidation state of Ce ions from Ce^{4+} to Ce^{3+} under reducing conditions that leads to the increase in the electronic conductivity. As a result, the material shows a significant electronic (polaron) conductivity counteracting the desired oxygen diffusion and thus, degrades the cell performance [3–6].

To prevail over the disadvantages caused by electronic conduction in the doped ceria electrolytes, compositional modifications based on homogeneous and heterogeneous doping have been investigated to expand the electrolytic domain of the electrolytes for the application in IT-SOFCs. Lubke and Wiemhofer and Navarro et al., reported the extension of the electrolytic domain for the gadolinium-doped ceria (CGO) electrolytes by co-doping Pr that acted as an electron traps [7,8]. Apart from homogeneous doping strategies, for some of ionic conductors, it has been reported that the existence of an inert heterogeneous phase in a conducting matrix can expand the electrolytic domain of doped ceria electrolytes. Chockalingam et al. reported the heterogeneously distributed phase, including manganese- or cobalt-doped alumina, which can be a good electron trapping sites in the CGO electrolyte and effectively expand the electrolytic domain of the CGO composite [9]. In addition, there are a few studies using stable LSGM as a heterogeneous phase in the Sm-doped ceria electrolytes to expand the electrolytic domain regions [10,11]. These results have verified that incorporation of a heterogeneous phase into the ceria-based electrolyte matrix can be one of the promising strategies to control the electrolytic domain with increase in the ionic conductivity or suppress the electronic conduction.

In this study, the composite electrolytes x mol% $La_{0.8}Sr_{0.2}Ga_{0.8}Mg_{0.2}O_{3-\delta}$ (LSGM)–$(100-x)$ mol% $Ce_{0.9}Gd_{0.1}O_{1.95}$ (CGO), where $x = 0$–50, were synthesized via a mechanical mixing followed by a solid state reaction. The influence of LSGM concentration on the electrolytic domain regions in the CGO electrolytes were investigated under different low oxygen partial pressures as a function of temperature.

* Corresponding author. Tel.: +82 42 350 4118; fax: +82 42 350 3310.
E-mail address: dkkim@kaist.ac.kr (D.K. Kim).
[1] Both these authors contributed equally to this work.

0925-8388/$ – see front matter © 2009 Elsevier B.V. All rights reserved.
doi:10.1016/j.jallcom.2009.10.207

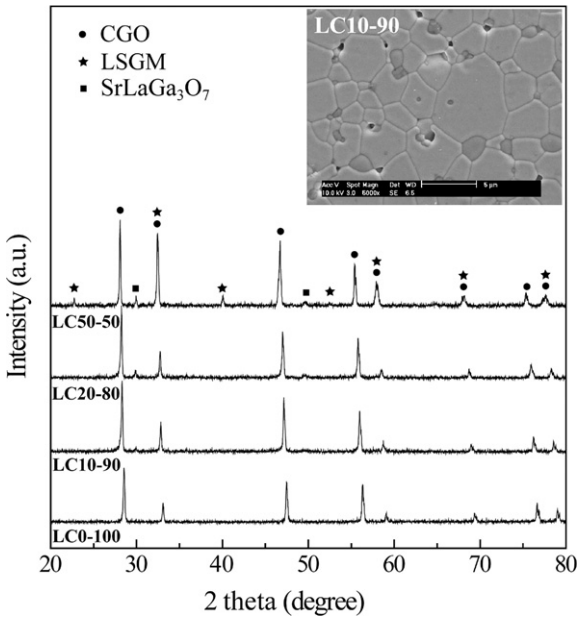

Fig. 1. X-ray diffraction patterns of the *x* mol% LSGM–CGO composites sintered at 1450 °C for 10 h. The inset shows SEM image of polished surface of the LC10-90 composites sintered at 1450 °C for 10 h.

2. Experimental

2.1. Preparation of composite electrolytes

The composite electrolytes of LSGM–CGO were prepared using synthesized LSGM powder and commercial 10 mol% Gd-doped ceria, $Ce_{0.9}Gd_{0.1}O_{1.95}$ (CGO) ultrafine powder (99.9% pure, Nextech Materials, USA) with particle size of ~5 nm and specific area of 176.5 $m^2\ g^{-1}$. According to the ICP (ICP-AES, OPTIMA 4300DV, Perkin Elmer, Yokohama, Japan) analysis, the most important impurities are: Si <20 ppm, Ca <20 ppm, K <100 ppm, Fe <35 ppm, Mg <53 ppm Al <41 ppm, Mn <2 ppm, Cr <15 ppm, Zn <3 ppm, Cu <3 ppm, and Ti <1 ppm. In a typical procedure, the $La_{0.8}Sr_{0.2}Ga_{0.8}Mg_{0.2}O_{3-\delta}$ (LSGM) powder was synthesized via a citric acid combustion method. Analytically pure $La(NO_3)_3{\cdot}6H_2O$, $Ga(NO_3)_3{\cdot}xH_2O$ (where $x = 10$ according to the analysis by elemental analysis), $Sr(NO_3)_2$, $Mg(NO_3)_2{\cdot}6H_2O$ (Aldrich Chemical Co., USA, 99.9%) were dissolved according to their respective molar ratios in warm distilled water (~50 °C). To a clear salts solution, a specific molar ratio of citric acid (Oriental Chemical Ind. Co.) was added under continuous stirring. The molar ratio of metal to citric acid was fixed at 1:1.8. The mixed solution was then heated at 90 °C on a hot plate under continuous magnetic stirring to form a polymeric gel, which was heated at 125 °C for 24 h in an oven to form swollen foam. The foam precursor was subjected to auto-combustion at ~250 °C. After the combustion, the precursor powder was ball-milled in *iso*-propanol with zirconia media and dried at 80 °C for 12 h in an oven. As-dried powder was calcined in an electrical furnace at 800 °C for 10 h to produce crystalline powder.

In a typical procedure, the above synthesized *x* mol% of LSGM powder calcined at 800 °C was thoroughly mixed with $(100 - x)$ mol% of commercial CGO nanopowder calcined at 800 °C for 10 h in an ethanolic medium. The dispersed LSGM–CGO powders were ball-milled for 24 h in ethanol using zirconia media. After subsequent drying and granulation, the powders were uniaxially pressed in a cylindrical stainless mold followed by cold isostatic pressure under 200 MPa. The LSGM–CGO pellets were sintered in an electric furnace at 1450 °C for 10 h in air with a heating ramp of 5 °C min^{-1}. The dispersed LSGM–CGO composite electrolytes in different *x* mol% of LSGM and CGO powders, where $x = 0$, 10, 20 and 50, and were denoted by the sample codes: LC0-100, LC10-90, LC20-80 and LC50-50.

2.2. Characterization of composite electrolytes

The phase compositions of the synthesized samples were characterized using an X-ray diffractometer (D/MAX-IIIC X-ray diffractometer, Rigaku, Tokyo, Japan) with Cu Kα radiation ($\lambda = 0.15406$ nm 40 kV and 45 mA). The XRD patterns were recorded for the pellets sintered at 1450 °C at a scan rate of 3 min^{-1}. The densification and grain morphology of the pellets for thermally etched polished surfaces of the sintered pellets were characterized using a scanning electron microscope (FE-SEM Philips XL30 FEG, Eindhoven, Netherland).

To perform impedance analysis, the surfaces of the sintered pellets were polished. Platinum paint was then applied to either side of the pellets, which were then heat-treated at 1000 °C for 1 h to facilitate stable contact of the electrode to the pellet surfaces. The platinum electrode-coated pellet was then attached to a platinum mesh, which was connected with platinum wires and sandwiched in a spring-loaded specimen holder. The electrical conductivity of the pellets was studied in the presence of air by alternating current (ac) impedance spectroscopy (Solartron 1260 impedance/Gain-phase analyzer, Farnborough, UK), which was interfaced with a computer controlled program for data acquisition. The impedance spectra were measured over the frequency range of 1 Hz to 10 MHz as a function of temperature from 250 °C to 900 °C in the presence of air, O_2/N_2 mixtures, and CO/CO_2 mixtures for the different oxygen partial pressures. The measurements were made for disc pellets below 600 °C in air and for bar pellets above 700 °C in the oxygen partial pressures of PO_2 10^{-33} to 1 atm.

3. Results and discussion

3.1. Phase formation and microstructures

The XRD patterns of the LC0-100, LC10-90, LC20-80 and LC50-50 composite pellets sintered at 1450 °C for 10 h are shown in Fig. 1. The XRD pattern of the LC50-50 sintered pellet clearly showed the presence of LSGM and CGO phases with an additional $SrLaGa_3O_7$ phase. However, LC10-90, LC20-80 pellets showed the presence of CGO phase with a trace amount of $SrLaGa_3O_7$ phase. The inset in Fig. 1 shows the SEM image of the polished and thermally

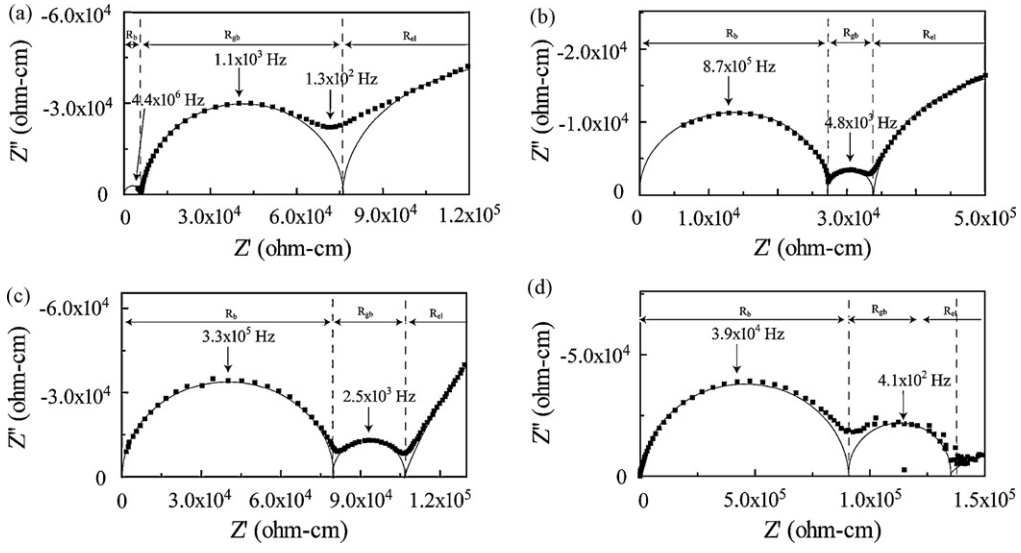

Fig. 2. Impedance spectra of (a) LC0-100, (b) LC10-90, (c) LC20-80 and (d) LC50-50 composites sintered at 1400 °C, measured at 250 °C.

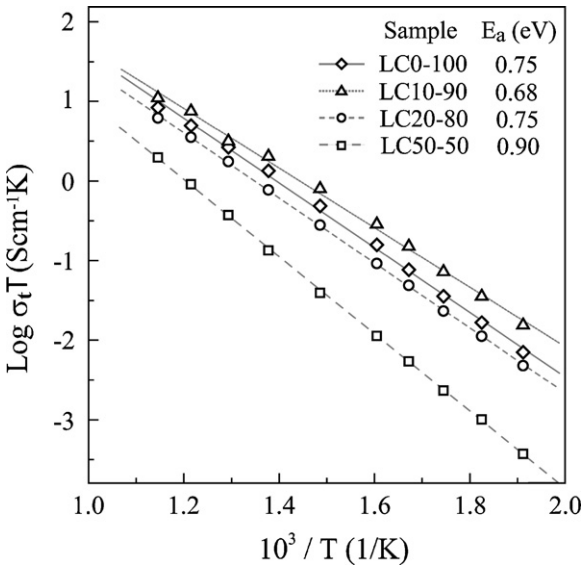

Fig. 3. Log $\sigma_t T$ versus 1000/T plots of the x mol% LSGM–CGO composites sintered at 1450 °C for 10 h.

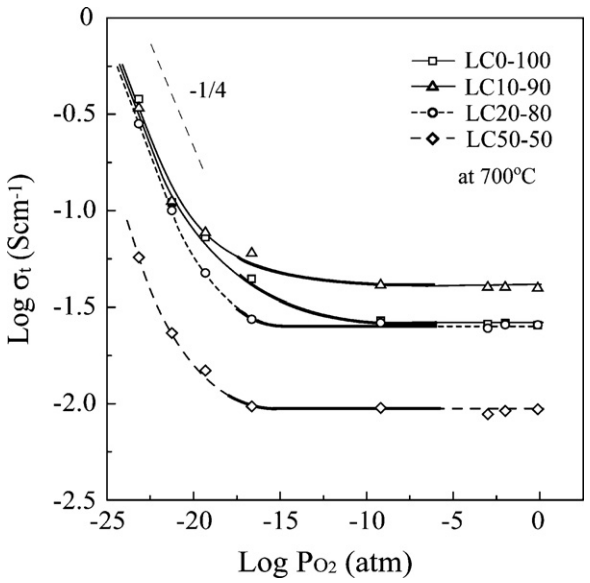

Fig. 4. Total electrical conductivities of the x mol% LSGM–CGO composites versus oxygen partial pressure, measured at 700 °C.

etched surface of the LC10-90 composite pellet sintered at 1450 °C. The micrograph images of sintered pellet revealed highly dense morphology with negligible porosity, and clearly resolved grain boundaries, which are typical microstructural features of highly sintered pellets.

3.2. Electrical transport properties

Fig. 2a–d shows the normalized complex impedance spectra with the sample geometry for the LC0-100, LC10-90, LC20-80 and LC50-50 composite pellets sintered at 1450 °C, measured at 250 °C. Also Fig. 2a–d shows the fit data and the plots identifying the resistivities attributed to the grain bulk, grain boundary and electrode responses. The presence of a dominant depressed semicircle at a high-frequency range is probably due to the resistivity of a grain bulk (R_b). The depressed semicircle in the middle-frequency region is due to the resistivity of a grain boundary (R_{gb}) response. The low-frequency region of the spectrum is attributed to the electrode resistivity (R_{el}). The detailed analyses of the impedance spectra with an equivalent circuit model are described in our previous reports [12]. The total resistivity (R_t) was obtained by fitting the impedance data with an equivalent circuit model using the non-linear least-squares fitting program of the *Z-view* software. As it is clear from the impedance spectra, the semicircles are depressed, and hence a constant phase element (CPE) is used instead of a pure capacitance. The impedance spectra were fit with an equivalent circuit model with two serial (R parallel with CPE) elements, of which one represents the bulk and the other is related with the grain boundary of the material. The electrode polarization at low-frequency can be modeled by a CPE_{el}. The total resistivity of the electrolyte is shown by $R_t = (R_b) + (R_{gb})$. Accordingly, the total electrical conductivity (σ_t) was calculated using the R_t of the samples. The bulk resistivity semicircles tend to enlarge as the concentration of LSGM was increased in the composite, which indicates a decrease in the bulk conductivity of the composite. On the other hand, relatively smaller grain boundary resistivity values were obtained for the composite pellet in comparison with a pure CGO pellet. It is evident to note that the addition of LSGM as a heterogeneous component in the CGO matrix significantly altered the impedance spectra of the CGO electrolytes.

Fig. 3 shows the calculated total electrical conductivity as a function of temperature following the Arrhenius equation $\sigma = A/T \exp(-E_a/k_b T)$, where A, E_a, and k_b are the pre-exponential factor, the activation energy, and Boltzmann constant, respectively. In Fig. 3, it is observed that the composite LC10-90 electrolyte exhibited the improved electrical conductivity and lower activation energy (0.68 eV) compared with pristine CGO, even though there is presence of trace amount of $SrLaGa_3O_7$ phase. The increase in the total conductivity for the LC10-90 electrolyte can be attributed to the reduction in grain boundary resistivity by presence of heterogeneous phases in the CGO matrix. On the other hand, the increase of LSGM concentration in the CGO matrix to 20 mol% (LC20-80) showed a slight lowering in the electrical conductivity, but its values were equivalent with those of pristine CGO. Further increment of LSGM (LC50-50) significantly impedes the electrical conductivity due to the dominant effect of the $SrLaGa_3O_7$ impurity phase.

Fig. 4 shows total electrical conductivities of the LC0-100, LC10-90, LC20-80 and LC50-50 composite pellets sintered at 1450 °C as a function of oxygen partial pressure (PO_2 10^{-33} to 10^{-1} atm), measured at 700 °C. The electrical conductivity of pristine CGO rapidly increased as the PO_2 decreased from 1 atm for a working temperature that followed a specific slope ($\partial \mathrm{Log}\,\sigma / \partial \mathrm{Log}\,PO_2$). The slope for pristine CGO is well known as −1/4. This oxygen pressure dependent conductivity behavior has been repeatedly observed for Gd-doped ceria [5,13,14] and is attributed to the constant ionic conductivity (σ_{ion}) due to oxygen vacancies whose concentration is fixed by that of the dopant Gd (i.e., $[Gd'_{Ce}] \approx 2[V^{\bullet\bullet}_O]$), followed by an increasing n-type conductivity (σ_n) with decreasing PO_2 [14]. The results shown in Fig. 4 suggest that the onset of the electronic conductivity is shifted towards more reducing conditions for the x mol% LSGM–CGO composite electrolytes. This suggests that the LSGM phase dispersed in the CGO matrix can be efficient to suppress the electronic conductivity at low PO_2 conditions. The results are represented as a bar diagram in Fig. 5, which shows the comparison of the electrical conductivities at 1 atm and 2.3×10^{-17} atm, measured at 700 °C. In which, the LC0-100 and LC10-90 showed an increase in the total electrical conductivity at 2.3×10^{-17} atm compared with the values measured at 1 atm, which is due to the contribution of electronic conductivity. However, LC20-80 and LC50-50 exhibited a steady plateau (Fig. 4) without any increase of electrical conductivity until at 2.3×10^{-17} atm, which can be attributed to the ionic mobility without any significant contribution of the electronic conductivity at low PO_2.

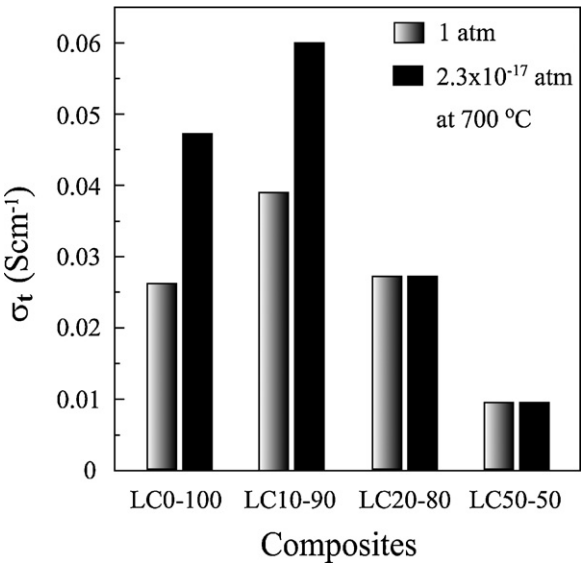

Fig. 5. Comparison of total electrical conductivity at 1 atm and 2.3×10^{-17} atm of *x* mol% LSGM–CGO composites, measured at 700 °C.

These results confirm the expanded electrolytic domain of the composite electrolytes of LC10-90 and LC-20-80 attributed to the compromising effects of the improved or retained ionic conductivity and the reduced electronic conductivity at low oxygen partial pressures. Thus, the composite electrolytes with the concentrations of LSGM phase in the CGO matrix have been revealed to facilitate improved ionic conductivity or relative reduced electronic conductivity at low PO_2 region, is proving to be a potential electrolyte for IT-SOFC.

4. Conclusion

The CGO-based composite electrolytes were synthesized by addition of the LSGM phase that coexists in the CGO matrix via the mechanical milling followed by solid state reaction. The composites were revealed to contain individual LSGM and CGO phases with a trace of $SrLaGa_3O_7$ phases. The specific composition of CGO composite with 10 mol% LSGM showed improved electrical conductivity compared to the pristine CGO electrolyte at overall temperature range, which is attributed to the increase in the grain boundary conductivity. The increased concentration of LSGM in the CGO matrix was effective to expand the electrolytic domain region with lowering an electronic conductivity compared to pristine CGO toward lower PO_2 region.

Acknowledgements

This work was financially supported by the Korea Research Foundation Grant funded by the Korean government (MOEHRD; KRF-2008-005-J00903). This work was also partially supported by Brain Korea 21 (BK21) program from Korean Ministry of Education.

References

[1] T. Ishihara, H. Matsuda, Y. Takita, J. Am. Chem. Soc. 116 (1994) 3801–3803.
[2] S.H. Jo, P. Muralidharan, D.K. Kim, Solid State Ionics 178 (2008) 1990–1997.
[3] B.C.H. Steele, Solid State Ionics 129 (2000) 95–110.
[4] H. Inaba, H. Tagawa, Solid State Ionics 83 (1996) 1–16.
[5] M. Mogensen, T. Lindegaard, U.R. Hansen, G. Mogensen, J. Electrochem. Soc. 141 (1994) 2122–2128.
[6] J.C.C. Abrantes, D. Pérez-Coll, P. Núñezb, J.R. Frade, Electrochim. Acta 48 (2003) 2761–2766.
[7] S. Lubke, H.D. Wiemhofer, Solid State Ionics 117 (1999) 229–243.
[8] L. Navarro, F. Marques, J. Frade, J. Electrochem. Soc. 144 (1997) 267–273.
[9] R. Chockalingam, V.R.W. Amarakoon, H. Giesche, J. Eur. Ceram. Soc. 28 (2008) 959–963.
[10] D. Xu, X. Liu, D. Wang, G. Yi, Y. Gao, D. Zhang, W. Su, J. Alloys Compd. 429 (2007) 292–295.
[11] D. Xu, X. Liu, C. Zuh, D. Wang, D. Yan, D. Wang, W. Su, J. Rare Earth 26 (2008) 241–244.
[12] S.H. Jo, P. Muralidharan, D.K. Kim, J. Mater. Res. 24 (2009) 237–244.
[13] S. Wang, T. Kobayashi, M. Dokiya, T. Hashimoto, J. Electrochem. Soc. 147 (2000) 3606–3609.
[14] S.H. Park, H.I. Yoo, Solid State Ionics 176 (2005) 1485–1490.